# High spatial resolution measurements of transverse stress in a fiber Bragg grating using four-state analysis low-coherence interferometry and layer-peeling*

R. Joseph Espejo and Shellee D. Dyer
National Institute of Standards and Technology
325 Broadway, Boulder, CO 80305 USA
Telephone: 303-497-7630, FAX: 303-497-7621,
Email: espejo@boulder.nist.gov

## ABSTRACT

Fiber Bragg grating (FBG) sensors have been shown to be a good means of nondestructive monitoring of the stress and/or strain of the materials in which they are embedded. Many FBG transverse stress/strain measurement systems can resolve only a single stress and/or strain value for the entire length of the FBG and often require the use of polarization-maintaining fiber. We demonstrate a new method for measuring the two components of transverse stress with high spatial resolution in a distributed FBG sensor. A directional compressive load is applied by placing weights on top of the FBG, creating a transverse stress in the core of the FBG. Small metallic strips are placed under the FBG to create a localized stress in the FBG. The relative index of refraction as a function of position in the FBG is determined with a low-coherence Michelson interferometer and a layer-peeling algorithm. With this method we are able to measure changes in the refractive index with resolution better than $5x10^{-6}$, limited by the signal-to-noise ratio of the measurement system, with a spatial resolution of 16 μm. To determine transverse stress, we repeat the measurement for four different polarization states. A four-state analysis is then used to determine the birefringence as a function of position in the grating. This measurement assumes that the applied transverse load is much larger than any other birefringence in the grating, so that the principal axes do not change with position in the grating. This measurement offers the advantage that it can be implemented with a simple layer-peeling algorithm, and it does not require the use of expensive polarization maintaining fiber. Measurements of the externally induced birefringence agree well with values predicted by the stress-optic properties and the geometry of the fiber.

**Keywords:** fiber Bragg gratings; fiber optic sensors; layer peeling; low coherence interferometry; transverse strain sensors.

## 1. INTRODUCTION

Over the past 10 years fiber Bragg gratings have come to play an important role in passive strain and stress detection. In the simplest form they are used as optical strain gauges. These devices are either attached to or imbedded in the host material that they are monitoring. As the host experiences strain, so does the optical fiber, which changes the grating period and thus the center wavelength of the reflected spectrum. The reflection spectrum is then monitored for shifts in wavelength, indicating a state of strain. The complete state of stress of the host material can be measured by embedding several of these strain gauge sensors in the host in orthogonal directions. This level of complexity can be difficult to implement, and the presence a large number of sensors may weaken the host. [1] The complete state of stress can be measured with a single FBG if a polarization sensitive measurement is used. The FBG can be written in polarization-maintaining fiber so that the wavelength along the two orthogonal polarization eigenstates can be monitored, giving information about the transverse strain. [2]



Smart Structures and Materials 2006: Smart Sensor Monitoring Systems and Applications,
edited by D. Inaudi, W. Ecke, B. Culshaw, K. J. Peters, E. Udd, Proc. of SPIE Vol. 6167
616707, (2006) · 0277-786X/06/$15 · doi: 10.1117/12.658061

Problems can arise if strains occur on scales smaller then the sensor's length, causing an uncertainty for inhomogeneous host materials such as composites. These sensors therefore must assume a constant stain across the entire length of the FBG, typically several millimeters, and are therefore limited to large-scale strain measurement.

In this paper we present a new method for interrogating a conventional FBG strain sensor that yields high spatial resolution, high sensitivity measurements of the transverse stress. The FBG is written in standard telecom single-mode fiber. Polarization information is obtained through a four-state analysis, so the system does not require any expensive polarization-maintaining fiber or devices. This makes it low cost and applicable to existing sensor systems. The high spatial resolution achieved by this method makes the sensor ideal for small-scale applications requiring high resolution, such as the testing of dental materials for microcracks and monitoring composite materials for internal delamination failures.

## 2. METHOD

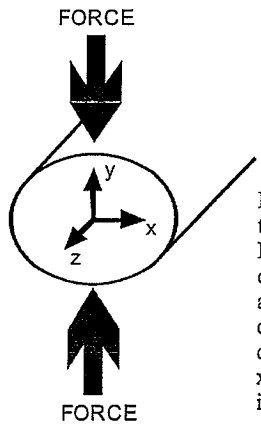


Figure. 1: Schematic showing the defined coordinate system. Force is applied in the y-direction. The fiber core lies along the z-axis. The force causes compression in the y-direction, and elongation in the x and z-directions (exaggerated in the drawing).

### 2.1 Stress in fibers

When the FBG is transversely compressed as in Fig. 1 stress in the direction of the applied force, $\sigma_y$, is negative due to compression. Stresses in the two orthogonal directions, $\sigma_x$ and $\sigma_z$, are positive. When the stress region is longer than the diameter of the fiber the stresses in the axial direction, $\sigma_z$, cancel, leaving only $\sigma_x$ and $\sigma_y$. In this paper we limit ourselves to this case so that axial elongations that would locally modify the grating's pitch are minimized. For a given compressive force these stresses are expressed in the Hertz equations [3]:

$$\begin{aligned} \sigma_x &= \frac{2F}{\pi DL}, \\ \sigma_y &= -\frac{6F}{\pi DL}, \\ \sigma_z &= 0. \end{aligned} \tag{1}$$

Here $D$ is the fiber diameter, $F$ is the applied force, and $L$ is the length of the region under stress.

The applied stress causes an anisotropic change in the refractive index, given by

$$\begin{aligned} \delta n_x &= -\frac{n_o^3}{2E}\left([p_{11}(1+\nu)(1-\nu) - p_{12}(1+\nu)\nu]\sigma_x + [p_{12}(1+\nu)(1-\nu) - p_{11}(1+\nu)\nu]\sigma_y\right) \\ &= C_1\sigma_x + C_2\sigma_y \\ \delta n_y &= -\frac{n_o^3}{2E}\left([p_{11}(1+\nu)(1-\nu) - p_{12}(1+\nu)\nu]\sigma_y + [p_{12}(1+\nu)(1-\nu) - p_{11}(1+\nu)\nu]\sigma_x\right) \\ &= C_2\sigma_x + C_1\sigma_y. \end{aligned} \tag{2}$$

The refractive index in the x and y-directions is then given by $n_x = n_o+\delta n_x$ and $n_y = n_o+\delta n_y$, with birefringence $\Delta n = \delta n_y - \delta n_x$. For the physical parameters of the fiber we use: $n_o = 1.47$ for the refractive index in the unstressed fiber core, $\nu = 0.17$ for the Poisson ratio, $E = 7.3\text{x}10^{10}$ Pa the Young's Modulus, and $p_{11} = 0.113$ and $p_{12} = 0.252$ are the strain-optic coefficients [2] [3]. The constants $C_1$ and $C_2$ are defined as the stress-optic coefficients.

### 2.2 FBG index reconstruction

For our sensor we require knowing the physical refractive index structure of the FBG, specifically the FBG's effective index. This is accomplished through the application of an inverse scattering algorithm known as layer-peeling to the measured complex reflection spectrum of the FBG.

The complex reflection spectrum is found by calculating the fast Fourier transform (FFT) of a measured interferogram, as described in Section 3.1. A layer-peeling algorithm is then applied to the calculated complex spectrum to determine the complex coupling coefficient of the FBG, $q(z)$ [4]. The index profile of a FBG can be described by its index modulation amplitude, $n_{ac}$, effective index, $n_{dc}$, and its Bragg period. These conventions used in this paper are analogous to those used to describe a signal waveform. It is important to note that the quantity $n_{dc}$ is not the absolute effective index, but rather the relative local change in the effective index from the mean value of the FBG.

The index modulation amplitude, $n_{ac}$, is calculated from $q(z)$ as follows:

$$n_{ac}(z) = \frac{|q(z)|\lambda_B}{\pi\eta}, \tag{3}$$

where $\lambda_B$ is the Bragg wavelength and $\eta$ is the fraction of power in the fiber core, taken from the manufacturer's specifications. The phase of the measured coupling coefficient can be related to the effective index, $n_{dc}$, by

$$\arg\big(q(z)\big) = \theta(z) - \frac{2\eta}{\lambda_B}\int_0^z n_{dc}(z')dz'. \tag{4}$$

Here, $|q(z)|$ is the vector magnitude of the coupling coefficient, and $\arg(q(z))$ is the corresponding phase angle. Assuming that the spatial grating phase, $\square(z)$, is constant, as is ideally the case for a FBG written with an un-chirped phase mask, the relative change in the average index, $n_{dc}$, can be found by differentiating $arg(q(z))$:

$$n_{dc}(z) = \frac{\lambda_B}{2\eta}\left(\frac{1}{\Lambda_B} - \frac{1}{\Lambda_{eff}(z)}\right). \tag{5}$$

Here, $\Lambda_B$ is the Bragg period, and the effective grating period $\Lambda_{eff}$ is determined from

$$\Lambda_{eff}(z) = \Lambda_B\left(1 + \frac{\Lambda_B}{2\pi}\frac{d}{dz}\arg(q(z))\right)^{-1}.$$

As a result of the assumption made for $\square(z)$ any deviation in the physical grating period, either from writing errors or environmental strain, will be interpreted as a change in $n_{dc}$.

A digital filter is applied to $arg(q(z))$ before differentiating for the purpose of reducing numerical differential noise. The pass-band of the filter must be carefully chosen so as to limit noise with out affecting the results; it must allow the highest measurable spatial frequency in the FBG spectrum to pass unaffected. Good results were typically found with the band-limit set though trial and error; reducing the band-limit to just before the spectrum is affected.

### 2.3 Four-state analysis

The 4-state algorithm is a powerful yet simple tool for gathering polarization information from a system that does not have a polarization maintaining ability. The algorithm was originally developed for measuring polarization dependent loss (PDL) and polarization mode dispersion (PMD) in optical fibers and components, and is also used to measure the polarization dependent wavelength shift (PDW) in FBGs [5-7]. In this paper we follow closely the method presented by [7], drawing on the relationship between PDW and the effective index.

In non-polarization maintaining fiber, a launched polarization state, ***S′***, can evolve in to another arbitrary polarization state, ***S***, as it travels through the fiber to the FBG. However, in the absence of polarization-dependent loss and depolarization, several distinct launch states will maintain their orientation relative to one another on the Poincaré sphere, as is shown in Fig. 2. This is because the states all see the same birefringent effects in the fiber and thus undergo the same unitary transformation.

A possible limitation of this method may be in the case of very high birefringence. The interferometric measurement requires that the polarization states in the reference and test arms of the interferometer are well matched for best fringe visibility. A strong birefringent rotation of the input state as it travels through the FBG will cause the fringe visibility to vary at different depths with in the FBG. This is an effective polarization dependent loss, which could potentially affect the results. In this paper we limit ourselves to nonbirefringent fiber and small loads so as to avoid these potential problems.

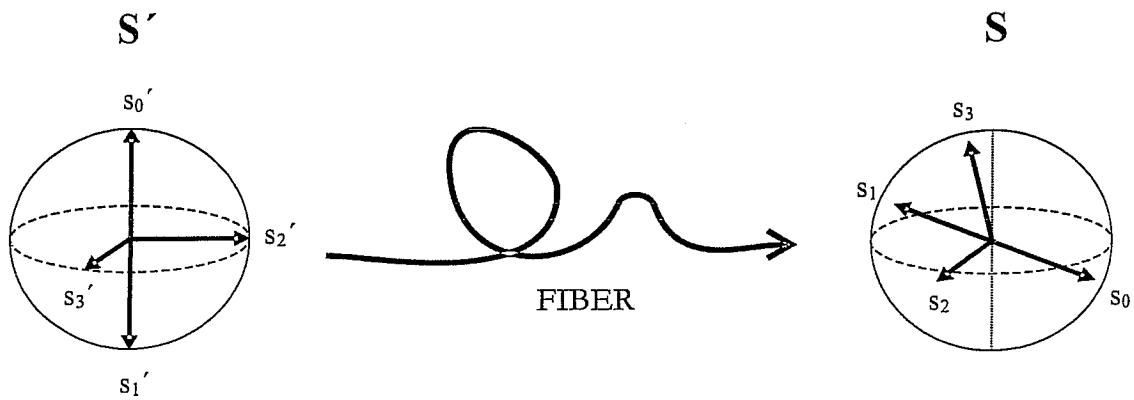


Figure 2: Schematic showing a length of fiber transforming the collection of states **S'** into arbitrary states **S**. The four launch states maintain their orientation with respect to each other as they propagate through the fiber.

The birefringence induced by transverse compression is directional, with the effective index having orthogonal eigenstates in the x and y directions. If we assume linear birefringence in the FBG, the effective index will vary sinusoidally as the polarization state moves between the two eigenaxes. The cross states, ± 45°, right-hand circular, and left-hand circular, occur midway between the two linear eigenstates and should therefore have same effective index. The value of the cross states is the average of the effective index of the eigenstates.

To facilitate the four-state calculation we define a modified Poincaré sphere. On this sphere the local birefringence in the FBG, $\Delta n$, is plotted on the surface instead of power, as is usually done. The polarization coordinate axes remain the same. Using this convention, the two orthogonal eigenaxes are mapped to the two linear states at the poles of the sphere. This is demonstrated in Fig. 3. Each measurement of $n_{dc}$ is the projection of the polarization vector at the grating on to the linear-state polar-axis of the Poincaré sphere, labeled **n** in Fig. 3b. On the sphere's geometry this can be expresses as $n_{dc} = \Delta n \cos(2\alpha)$.

Four states are needed to define the sphere, two of which are an orthogonal pair. The four states form a Mueller Set: three lie on a great circle on the sphere separated by 90°, and the fourth is on the axis of the great circle. Two of these

states form an orthogonal pair. For convenience we chose 0°, 90°, + 45°, and right-hand circular for the input states, $s_0'$, $s_1'$, $s_2'$, and $s_3'$, of S′.

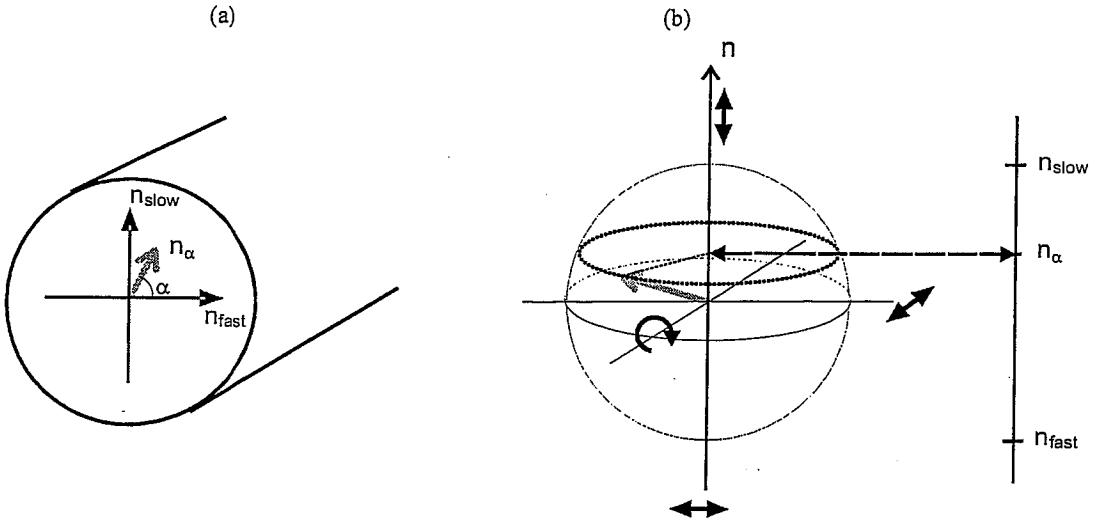


Figure 3: (a): A polarization state propagating through the fiber at angle α with respect to the eigenaxis will see an effective index $n_\alpha$ (b): The polarization state expressed on a modified Poincaré sphere. The eigenaxes are mapped to the horizontal-vertical states axis, labeled **n**. Refractive index as a function of angle α is then mapped as a projection on to this axis.

To calculate $\Delta n$, which is the diameter of the sphere, we define the quantities,

$$\overline{n} = \frac{n_{s0} + n_{s1}}{2},$$

where $n_{s0}$ and $n_{s1}$ are the orthogonal pair of states, and

$$\delta n_{si} = \frac{\Delta n}{2}\cos\phi_{si} = n_{si} - \overline{n}; \quad i = 0,1,2,3.$$

The value of $\overline{n}$ will always lie on the equator of the sphere, regardless of the orientation of the states $s_0$ and $s_1$, since $s_0$ and $s_1$ are an orthogonal pair. The birefringence is then given by

$$\Delta n = 2\sqrt{\delta n_{s1}{}^2 + \delta n_{s2}{}^2 + \delta n_{s3}{}^2}. \qquad (6)$$

The $n_{dc}$ values of the two eigenstates can then be expressed as $n_{dc}^{fast} = \overline{n} - \Delta n$ and $n_{dc}^{slow} = \overline{n} + \Delta n$.

## 3. EXPERIMENTAL SETUP

### 3.1 Low-coherence interferometer

We use low-coherence interferometry (LCI) to measure the impulse response of the grating. The impulse response of the FBG is measured using the fiber-optic Michelson LCI, shown in Fig. 4. We have previously shown that accurate, high-resolution measurements of the dispersive and spectral properties of optical components can be achieved using this measurement system [8]. A layer-peeling algorithm is then used to calculate the complex spatial coupling coefficient of the FBG. From the coupling coefficient we can then find the longitudinal refractive index and phase of the FBG.

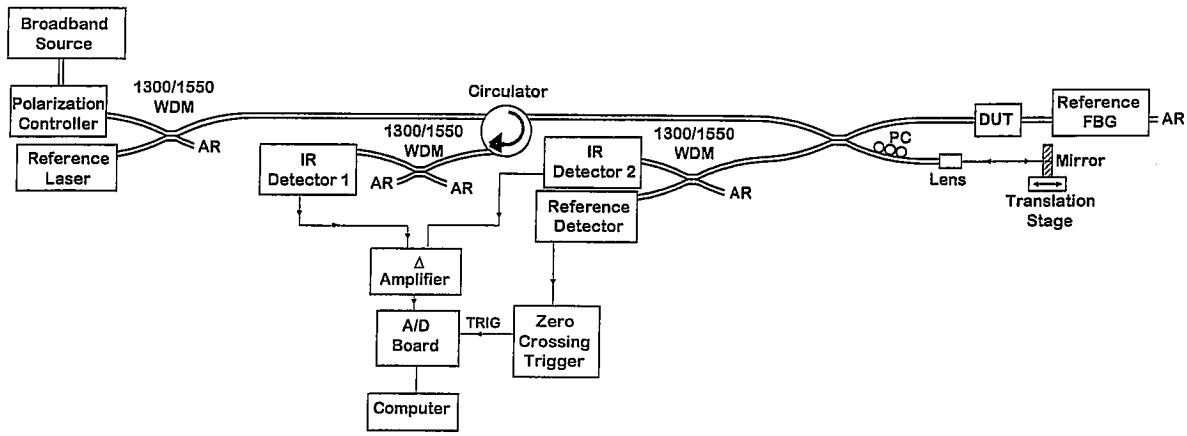


Figure 4. Low-coherence measurement system. DUT: device under test. AR: anti-reflection. PC: polarization control, for matching the polarization state of the two arms. WDM: wavelength division multiplexer.

The FBG to be measured (DUT) is placed in one arm of the Michelson LCI along with a 1319 nm reference grating. The reference arm of the interferometer has a variable air path that is capable of scanning a total optical path distance of 1.4 m. The low-coherence illumination is provided by a commercial C+L band superfluorescent source with a 3 dB bandwidth of 85 nm centered at 1565 nm. The polarization launch states for the low-coherence light are set with a polarization controller. A 1319 nm Nd:YAG reference laser tracks the interferometer's total optical path difference as the reference arm mirror is translated. The reference grating provides a narrowband reflection of just the reference laser signal. The low-coherence signal is differentially detected and then digitized with a 16-bit A/D card. Triggering occurs at every zero crossing of the interference signal created by the reference laser, which sets the sample spacing to 659.5 nm. The signal-to-noise ratio (SNR) is greater than 70 dB (20 Log of detector current), measured as the signal peak over the standard deviation of the noise.

The localized index changes in the FBG that are induced by external stress often result in a reflection spectrum with very fine spectral details. Such a spectrum will have a very long impulse response. When measuring these gratings with our interferometric system, we find it necessary to scan over a very long length to accurately capture the interferogram. Typical scan lengths are $2^{19}$ data points, or about 35 cm of scan mirror travel. Shorter scans can result in a spectrum that is distorted by the smoothing of these fine spectral features.

The spatial resolution of the calculated FBG index profile is inversely related to the bandwidth of the low-coherence source [3]. A spectral range from 1525 nm to 1610 nm gives a maximum longitudinal spatial resolution for the FBG sensor of 15 μm inside the fiber.

### 3.2 Fiber loading fixture

Transverse loads are applied to the FBG using the fixture shown in Fig. 5. With this fixture a known compressive force can be applied to the FBG in a controlled manner by placing weights on top of the fixture. The fixture is thermally stabilized with a temperature controlled thermal-electric cooler (TEC) in order to isolate the FBG from the effects of thermal variations. The FBG is also mounted so as to minimize the transfer of external stress onto the FBG. These measures effectively isolate the FBG environmental fluctuations, so that only the applied transverse stress is present in the measurement. The test FBG and a support fiber are sandwiched between two thick polished glass plates. The support fiber ensures that the plates are parallel so that the compressive force is always perpendicular to the plates.

A metal pin is placed between the upper glass plate and the aluminum top plate, centered between the two fibers. This is to prevent torsion of the load, and to evenly distribute the load between the two fibers. In this configuration the force applied to the FBG is $mg/2$; $m$ is the applied mass, and $g$ is the gravitational constant. Two screws are used to hold the top plate in place and keep it from rotating out of position when the weights are added. The screws are left loose so as

not to add any compression. The weights are balanced directly above the pin so that the screws affect the load as little as possible.

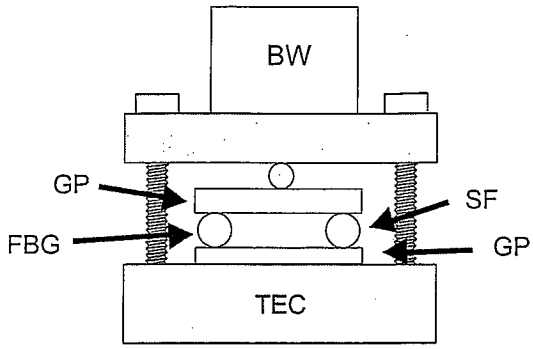


Figure. 5: Schematic of the fiber loading fixture. SF: support fiber; GP: glass plate; BW: brass weight; TEC: thermal-electric cooler.

## 4. RESULTS

We used a 2.5 cm long FBG written in a common nonbirefringent single mode fiber that had been previously hydrogen-loaded. The hydrogen-loading was done to increase photosensitivity when writing the FBG. The FBG has a peak reflectivity of 15.5 dB at 1538.5 nm. The jacket was stripped from both the FBG and the support fibers. This is out of concern that permanent deformation of the soft jacket material caused by loading pressures might affect or influence later measurements in an unpredictable manner.

A 500 μm wide aluminum strip was placed under the FGB in the loading fixture to produce a localized transverse stress. The FBG was measured with the low-coherence system and the birefringence, $\Delta n$, was found with the layer-peeling and four-state algorithms; the results are plotted in Fig. 6. The peak birefringence agrees with the values predicted by the Hertz equations. We found the sensor to be very sensitive to even small applied loads, including the 15 gram load placed by the unladen fixture.

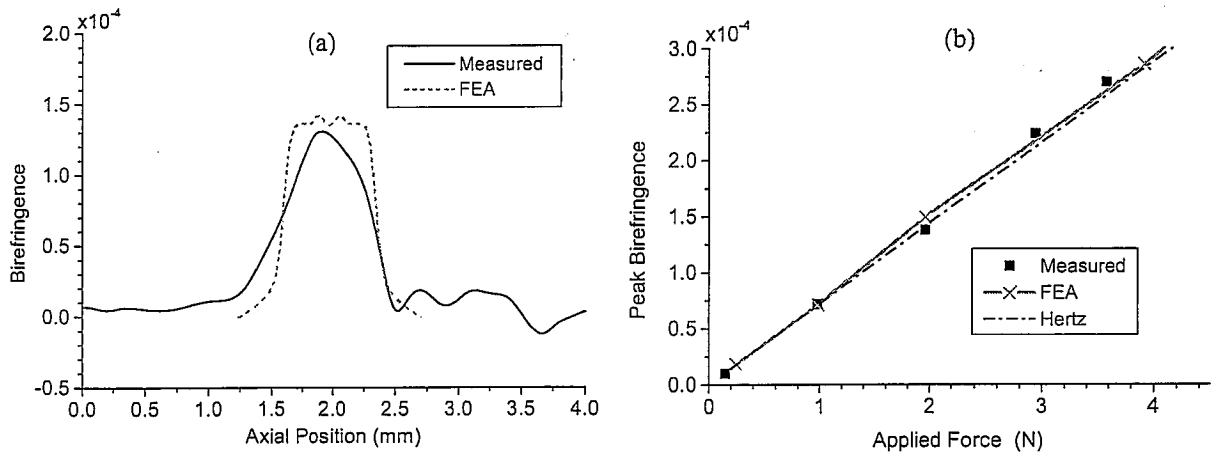


Figure 6: (a) Measured and calculated birefringence in the core of the FBG near the location of the metal strip. (b) The peak value of the birefringence in plot (a) for several different applied forces. FEA: finite element analysis.

A finite element analysis model (FEA) was used to predict and verify the measured transverse stress in the FBG. The fiber was modeled as a solid cylinder of fused silica. The cylinder was then placed under a localized compressive load by a metallic block of length L. The transverse stress values were computed along the axis of the cylinder, simulating the

stress in the core of the FBG sensor. The FEA stress was calculated for a 500 μm wide block with the applied forces used in the measurement. There is good agreement between the measured birefringence and predicted by FEA and equations (2). The measured birefringence profile in Fig. 6a matches the FEA profile reasonably well in terms of overall width and height. The cause for the difference in shape is not fully understood, but is most likely caused by improper coupling between the aluminum strip and the FBG. The sensor displays a higher accuracy at smaller applied force.

## 5. CONCLUSIONS

We have demonstrated a fiber Bragg grating sensor system capable of measuring transverse stress with high spatial resolution. Standard telecom single-mode components are used in the system, making it low-cost. Measurements performed on a diametrically compressed grating agree very well with stress predicted by the Hertz plane-stress equations as well as finite element modeling.

## REFERENCES


1. E. Udd, "An overview of fiber optic sensors," *Rev. Sci. Instrum.*, vol. 66 no. 8, pp. 4015-4030, 1995.

2. C.M. Lawrence, D.V. Nelson, E. Udd and T. Bennett, "A fiber optic sensor for transverse strain measurement," *Exp. Mech.*, vol. 39, no. 3, pp. 202-209, 1999.

3. R.B. Wagreich, E.A. Altia, H. Singh, and J.S. Sirkis "Effects of diametric load on fibre Bragg gratings in low birefringence fibre," *Elect. Lett.*, vol. 32, no. 13, pp. 1223-1224, 1996.

4. J. Skaar, L. Wang, and T. Erdogan, "On the Synthesis of Fiber Bragg Gratings by Layer Peeling," *IEEE J. Quan. Elect.*, vol.37, no. 2, pp. 165-173, 2001.

5. R.M. Craig, S.L. Gilbert, and P.D. Hale, "High-Resolution, Nonmechanical Approach to Polarization-Dependent Transmission Measurements," *J. Light. Tech.*, vol. 16, no. 7, 1998.

6. P.A. Williams, "Modulation phase-shift measurement of PMD using only four launched polarisation states: a new algorithm," *Elect. Lett.*, vol. 35, no. 18, pp. 1578-1579, 1999.

7. W.C. Swann, S.D. Dyer, R.M. Craig, "Four-state measurement method for polarization dependent wavelength shift," SOFM 2002, Boulder, CO, NIST Spec. Publ. 988, pp. 125-128, 2002.

8. S.D. Dyer, R.J. Espejo, and P.A. Williams, "High-Resolution Group Delay Measurements of a Hydrogen Cyanide Gas Cell Using Low-Coherence Interferometry," SOFM 2002, Boulder, CO, NIST Spec. Publ. 988, pp. 45-48, 2002.